International Journal of Heat and Fluid Flow 50 (2014) 63–71

Contents lists available at ScienceDirect

International Journal of Heat and Fluid Flow

journal homepage: www.elsevier.com/locate/ijhff

Dynamics of a compound droplet in shear flow

Haobo Hua [a,b], Jaemin Shin [c], Junseok Kim [a,*]

[a] Department of Mathematics, Korea University, Seoul 136-713, Republic of Korea
[b] School of Mechanical & Aerospace Engineering, Nanyang Technological University, Singapore 639798, Singapore
[c] Institute of Mathematical Sciences, Ewha W. University, Seoul 120-750, Republic of Korea

ARTICLE INFO

Article history:
Received 25 November 2013
Received in revised form 26 March 2014
Accepted 13 May 2014
Available online 11 June 2014

Keywords:
Compound droplet
Immersed boundary method
Shear flow
Drop deformation

ABSTRACT

The deformation dynamics of a compound liquid droplet in shear flow is numerically investigated in two- and three-dimensional space. The computational model is based on the immersed boundary method. This accurately and efficiently tracks the interfaces of immiscible multi-phase fluids. We extend a recently developed volume-conserving immersed boundary method for two-phase fluid flow to ternary compound droplet flows. For long time simulations, we also apply a surface remeshing algorithm. Chorin's projection method is employed, and the resulting system of discrete equations is solved by a multigrid technique. We study the effects of radius, interfacial tension ratios, and inner droplet location on the deformation of a compound droplet, and compute the inclination angles of inner and outer droplets. Simulation results indicate that the angle of the inner droplet is always greater than or equal to that of the outer one. The effect of wall confinement on compound droplet deformation is compared with that of a simple droplet. The result shows that the more confined the wall is, the more different the compound and simple droplets' behavior.

1. Introduction

The dynamics of multiphase droplets is of great interest in many fields of science and technology. The hydrodynamics of simple droplets and blends under various flow conditions has been intensively investigated from theoretical (Hinch and Acrivos, 1980; Taylor, 1934), computational (Renardy and Cristini, 2001; Renardy, 2007; Janssen and Anderson, 2007; Vananroye et al., 2008; Yue et al., 2004, 2006; Pillapakkam and Singh, 2001; Sheth and Pozrikidis, 1995; Hua et al., 2013), and experimental (Rumscheidt and Mason, 1961; Torza et al., 1972; Bartok and Mason, 1959) perspectives. The growing interest in the generation and manipulation of compound droplets is mainly due to microfluidic applications (Utada et al., 2005; Chen et al., 2007; Hirofumi et al., 2007). For example, Utada et al. (2005) fabricated double emulsions that contained a single internal droplet in a core–shell geometry using a microcapillary device.

Johnson and Sadhal (1985) reviewed the fluid mechanics of compound multiphase droplets in the static state and their translation in quiescent flow. The behavior of double emulsion droplets in extensional flows was analytically studied in (Stone and Leal, 1990), and Bazhlekov et al. (1995) numerically studied the unsteady motion of a rising compound droplet in a viscous fluid under the effect of gravity using the finite element method. Smith et al. (2004) investigated the deformation and breakup of an encapsulated droplet in shear flow using the level set method. They focused on the recovery behavior of an equiviscous compound droplet, and presented a phase diagram to describe the morphologies for a range of capillary numbers and surface tensions. As a first step to develop a model for the deposition of a cell-encapsulating droplet, Tasoglu et al. (2010) studied the impact and spreading of a compound viscous droplet on a flat surface using the front-tracking method. Gao and Feng (2011) developed a diffuse-interface method to simulate the spreading and breakup of a compound drop on a partially wetting substrate. They observed three regimes for the interfacial behavior, mainly depending on the size of the inner droplet. Recently, Qu and Wang (2012) studied the hydrodynamics of concentric and eccentric compound droplets in extensional flows using the spectral boundary element method. They explored parameter effects in detail, including the relative size and surface tension of two interfaces, the capillary number, and the initial location of an inner droplet in the compound droplet, on the deformation and stability of the compound droplet in the Stokes flow regime. There are several experimental (Vananroye et al., 2007; Sibillo et al., 2006) and numerical (Renardy, 2007; Janssen and Anderson, 2007; Vananroye et al., 2008) results for the confinement effect on the

* Corresponding author. Tel.: +82 2 3290 3077; fax: +82 2 929 8562.
E-mail addresses: hbhua@ntu.edu.sg (H. Hua), zmshin@korea.ac.kr (J. Shin), cfdkim@korea.ac.kr (J. Kim).
URL: http://math.korea.ac.kr/~cfdkim (J. Kim).

http://dx.doi.org/10.1016/j.ijheatfluidflow.2014.05.007
0142-727X/

steady-state shape of a simple droplet under shear flow. The phenomenological models make an important contribution to our comprehension of the deformation and breakup of a single droplet (Minale, 2008, 2010). However, there are no numerical results for the wall effect with respect to a compound droplet.

The novel contributions of this study are as follows: (i) we extend the three-dimensional volume-conserving immersed boundary method and apply surface remeshing for a compound droplet; (ii) the influence of fluid properties, droplet size, and inner droplet location are investigated; and (iii) the wall confinement effect is also studied and compared with a simple droplet. The rest of the paper is organized as follows. In Section 2, the mathematical governing equations are introduced. In Section 3, we describe the numerical implementation in detail. The results of numerical simulations are presented in Section 4. Finally, conclusions are drawn in Section 5.

2. Governing equations

We study the two- and three-dimensional dynamics of a compound liquid droplet suspended in an ambient fluid between two parallel plates under a shear flow with shear rate $\dot{\gamma}$, as schematically illustrated in Fig. 1. The domains Ω_1, Ω_2, and Ω_3 represent the inner, outer, and ambient fluids, respectively, and Γ_m denotes the interface between fluids Ω_m and Ω_{m+1} $(m = 1, 2)$. σ_m is the surface tension coefficient on Γ_m, and ρ_m and μ_m are density and viscosity, respectively, in Ω_m. For simplicity, we consider constant density and viscosity.

In each fluid, the Navier–Stokes and continuity equations are satisfied

$$\rho_m\left(\frac{\partial \mathbf{u}_m}{\partial t} + \mathbf{u}_m \cdot \nabla \mathbf{u}_m\right) = -\nabla p_m + \mu_m \Delta \mathbf{u}_m, \quad \text{for } m = 1, 2, 3, \tag{1}$$

$$\nabla \cdot \mathbf{u}_m = 0, \tag{2}$$

where $\mathbf{u}_m = \mathbf{u}_m(\mathbf{x}, t)$ is the fluid velocity and $p_m = p_m(\mathbf{x}, t)$ is the pressure field, defined for the Cartesian coordinate $\mathbf{x} \in \Omega_m$ at time t. The velocity is continuous across the droplet interface Γ_m, and the normal stress jump is balanced by the interfacial force $\mathbf{f}_m$, i.e., $[-p\mathbf{I}\mathbf{n}_m + \mu\nabla\mathbf{u}\mathbf{n}_m]_{\Gamma_m} + \mathbf{f}_m = 0$, where $\mathbf{n}_m$ is the unit normal vector on Γ_m. However, it is not easy to solve Eqs. (1) and (2) directly with jump conditions at the interfaces. To overcome these difficulties, we use the immersed boundary method (IBM), which was developed by Peskin (1977). In IBM, we treat the interface as an immersed boundary that exerts a force $\mathbf{f}$ on the fluids and moves with the local fluid velocity (Lai et al., 2008).

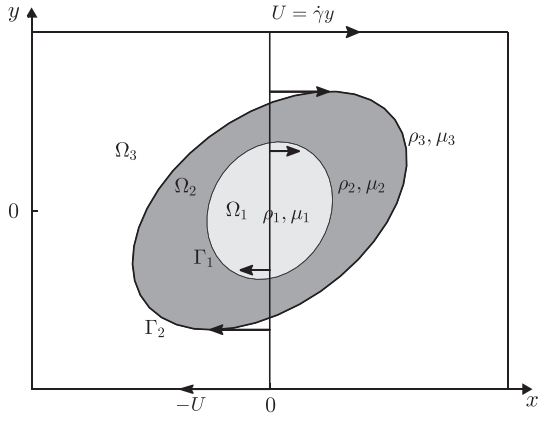

Fig. 1. Compound droplet in an ambient fluid under shear flow.

We denote by $\mathbf{X}_m(t)$ the Lagrangian variable for the immersed boundary $\Gamma_m, m = 1, 2$. The fluid flow is computed in the whole domain, and then $\mathbf{X}_m(t)$ is moved according to the interpolated fluid velocity. The fluid interacts with the interface through the surface tension force exerted by the boundary. This surface tension force is spread to the surrounding Eulerian variable $\mathbf{x}$ using a delta function. Then, the dimensionless equations of motion for the system of immiscible three-phase fluid flow can be written in the following form:

$$\frac{\partial \mathbf{u}(\mathbf{x}, t)}{\partial t} + \mathbf{u}(\mathbf{x}, t) \cdot \nabla \mathbf{u}(\mathbf{x}, t) = -\nabla p(\mathbf{x}, t) + \frac{1}{Re}\Delta \mathbf{u}(\mathbf{x}, t) + \mathbf{f}(\mathbf{x}, t), \tag{3}$$

$$\nabla \cdot \mathbf{u}(\mathbf{x}, t) = 0, \tag{4}$$

$$\mathbf{f}(\mathbf{x}, t) = \sum_{m=1}^{2} \frac{1}{We_m} \mathbf{f}_m(\mathbf{x}, t), \tag{5}$$

$$\mathbf{f}_m(\mathbf{x}, t) = \int_{\Gamma_m} \mathbf{F}_m(\mathbf{X}_m(t))\delta(\mathbf{x} - \mathbf{X}_m(t))ds, \tag{6}$$

$$\frac{d\mathbf{X}_m(t)}{dt} = \mathbf{U}_m(\mathbf{X}_m(t)) \quad \text{for } m = 1, 2, \tag{7}$$

$$\mathbf{U}_m(\mathbf{X}_m(t)) = \int_{\Omega} \mathbf{u}(\mathbf{x}, t)\delta(\mathbf{x} - \mathbf{X}_m(t))d\mathbf{x}. \tag{8}$$

Here, $\mathbf{u}(\mathbf{x}, t)$, $p(\mathbf{x}, t)$, $\mathbf{f}_m(\mathbf{x}, t)$ are Eulerian variables and $\mathbf{F}_m(\mathbf{X}_m(t))$, $\mathbf{U}_m(\mathbf{X}_m(t))$ are Lagrangian variables in the Cartesian domain $\Omega \subset \mathbb{R}^d$ ($d = 2$ or 3). The Lagrangian force density is defined as $\mathbf{F}_m(\mathbf{X}_m(t)) = \kappa_m(\mathbf{X}_m(t))\mathbf{n}_m(\mathbf{X}_m(t))$, where κ_m is the mean curvature and $\mathbf{n}_m$ is the unit outward normal vector at the interface Γ_m. $\delta(\mathbf{x})$ is the Dirac delta function defined as the product of one-dimensional Dirac delta functions, i.e., $\delta(\mathbf{x}) = \delta(x)\delta(y)$ and $\delta(\mathbf{x}) = \delta(x)\delta(y)\delta(z)$ in two and three dimensions, respectively.

Let R_1 and R_2 be the undeformed radii of the inner and outer droplets, respectively. The length scale is R_2. $1/\dot{\gamma}$ is the time scale, where $\dot{\gamma}$ is the shear rate. Thus, $\dot{\gamma}R_2$ is the velocity scale. We now define the capillary numbers $Ca_m = \mu_3\dot{\gamma}R_m/\sigma_m$ for the inner $(m = 1)$ and outer $(m = 2)$ droplets. Other dimensionless parameters are the Reynolds number $Re = \rho_3\dot{\gamma}R_2^2/\mu_3$ and the interface-specific Weber numbers $We_m = Ca_m Re$. For the computational domains, we use $\Omega = (-L_x, L_x) \times (-L_y, L_y)$ and $\Omega = (-L_x, L_x) \times (-L_y, L_y) \times (-L_z, L_z)$ for two- and three-dimensional spaces, respectively. The initial conditions are $(u, v) = (y, 0)$ and $(u, v, w) = (z, 0, 0)$. The boundary conditions are $u(x, L_y) = -u(x, -L_y) = L_y$, $v(x, L_y) = v(x, -L_y) = 0$, and $u(x, y, L_z) = -u(x, y, -L_z) = L_z$, $v(x, y, L_z) = v(x, y, -L_z) = w(x, y, L_z) = w(x, y, -L_z) = 0$. For the pressure field, we take the homogeneous Neumann boundary condition at the top and bottom plates. In the other directions, we use periodic boundary conditions.

3. Numerical solution

In this section, we briefly describe the numerical solutions for IBM in three dimensions. Volume-conserving and remeshing algorithms are used to preserve the mass of the droplet and maintain a high-quality surface mesh.

3.1. Discretization

We discretize the domain $\Omega = (-L_x, L_x) \times (-L_y, L_y) \times (-L_z, L_z)$ in three-dimensional space. Two-dimensional discretization is analogously defined. Let the computational domain be partitioned into a uniform mesh with a space step of size h in a Cartesian geometry. The center of each cell is located at $\mathbf{x}_{ijk} = (x_i, y_j, z_k)$, where

$x_i = -L_x + (i-0.5)h$, $y_j = -L_y + (j-0.5)h$, and $z_k = -L_z + (k-0.5)h$, for $i = 1,\ldots,N_x$, $j = 1,\ldots,N_y$, and $k = 1,\ldots,N_z$. N_x, N_y, and N_z are the numbers of cells in the x-, y-, and z-directions, respectively. Let u^n_{ijk} be an approximation of $u(\mathbf{x}_{ijk}, t_n)$, where $t_n = n\Delta t$ and Δt is the time step size. We use a staggered marker-and-cell mesh (Harlow and Welch, 1965), in which pressure is stored at the cell centers and the velocity components u, v, and w are defined at the x-, y-, and z-directional face centers, respectively (see Fig. 2(a)). We use a set of M_m Lagrangian points $\mathbf{X}^n_{m,l} = (X^n_{m,l}, Y^n_{m,l}, Z^n_{m,l})$ for $l = 1,\ldots,M_m$ to discretize the immersed boundary Γ_m (see Fig. 2(b)).

3.2. Immersed boundary method

At the n-th time step, we have a divergence-free velocity field $\mathbf{u}^n$ and a surface tension force $\mathbf{f}^n$ calculated from the boundary configuration $\mathbf{X}^n$. An outline of the main procedure in one time step containing the volume correction and remeshing algorithms is as follows:

Step 1. Surface tension force
From the inner ($\mathbf{X}^n_{1,l}$ for $l = 1,\ldots,M_1$) and outer ($\mathbf{X}^n_{2,l}$ for $l = 1,\ldots,M_2$) droplet boundary configurations, we calculate the boundary force densities.

$$\mathbf{F}^n_{m,l} = \kappa^n_{m,l}\mathbf{n}^n_{m,l}, \quad \text{for } m = 1,2 \text{ and } l = 1,\ldots,M_m, \tag{9}$$

where $\kappa^n_{m,l}$ is the mean curvature and $\mathbf{n}^n_{m,l}$ is the normal vector at $\mathbf{X}^n_{m,l}$. We then calculate the surface tension force,

$$\mathbf{f}^n_{ijk} = \sum_{m=1}^{2}\left[\frac{1}{We_m}\sum\nolimits_{l=1}^{M_m}\mathbf{F}^n_{m,l}\delta_h(\mathbf{x}_{ijk} - \mathbf{X}^n_{m,l})\Delta\mathcal{A}_{m,l}\right], \tag{10}$$

for $i = 1,\ldots,N_x$, $j = 1,\ldots,N_y$, and $k = 1,\ldots,N_z$, where δ_h is a smoothed Dirac delta function (Peskin and McQueen, 1995) and $\Delta\mathcal{A}_{m,l}$ is a surface area element for each interface. Refer to (Li et al., 2013) for details of the curvature and normal vector calculations.

Step 2. Velocity update
The Navier–Stokes Eqs. (3) and (4) are solved by the projection method (Choirn, 1968). First, we solve for an intermediate velocity $\tilde{\mathbf{u}}$,

$$\frac{\tilde{\mathbf{u}} - \mathbf{u}^n}{\Delta t} + \mathbf{u}^n \cdot \nabla_d \mathbf{u}^n = \frac{1}{Re}\Delta_d \mathbf{u}^n + \mathbf{f}^n, \tag{11}$$

where ∇_d and Δ_d denote the centered difference approximations for the gradient and Laplacian operators, respectively. Second, we solve the following equation for the pressure field

$$\Delta_d p^{n+1} = \frac{1}{\Delta t}\nabla_d \cdot \tilde{\mathbf{u}}, \tag{12}$$

where $\nabla_d \cdot$ denotes the discrete divergence operator. The resulting system of Eq. (12) is solved using a multigrid method (Trottenberg et al., 2001). The velocity field $\mathbf{u}^{n+1}$ is then computed by

$$\mathbf{u}^{n+1} = \tilde{\mathbf{u}} - \Delta t \nabla_d p^{n+1}. \tag{13}$$

Step 3. Interface marker position update
The new immersed boundary positions are computed from the updated velocity field:

$$\mathbf{X}^{n+1}_{m,l} = \mathbf{X}^n_{m,l} + \Delta t \mathbf{U}^{n+1}_{m,l}, \quad \text{for } m = 1,2, \text{ and } l = 1,\ldots,M_m, \tag{14}$$

$$\text{where } \mathbf{U}^{n+1}_{m,l} = \sum_{i=1}^{N_x}\sum_{j=1}^{N_y}\sum_{k=1}^{N_z}\mathbf{u}^{n+1}_{ijk}\delta_h(\mathbf{x}_{ijk} - \mathbf{X}^n_{m,l})h^3. \tag{15}$$

Steps 1–3 complete the procedure for calculating the fluid velocity $\mathbf{u}^{n+1}$ and boundary position $\mathbf{X}^{n+1}$. We then apply the volume-conserving algorithm (Li et al., 2013) and remeshing procedure to $\mathbf{X}^{n+1}$ to preserve the initial volume and high-quality surface mesh (Hua et al., 2013), respectively.

4. Numerical experiments

4.1. Pressure jump

In the absence of viscous, gravitational, and other external forces, the pressure gradient is balanced by the surface tension force. Using Laplace's formula for an infinite cylindrical liquid surrounded by an ambient fluid at zero pressure, the pressure difference is $[p]_\Gamma = \sigma/R$, where R is the droplet radius and σ is the surface tension coefficient of the interface Γ (Landau and Lifshitz, 1987). We consider the equilibrium of a drop-in-drop placed within another fluid (see Fig. 3(a)) in two dimensions. Thus $[p]_{\Gamma_m} = \sigma_m/R_m$, where σ_m and R_m are the surface tension coefficient and droplet radius of the interface Γ_m for $m = 1,2$, respectively. The initial conditions are circles with $R_1 = 0.2$ and $R_2 = 0.4$. The surface tension coefficients are $\sigma_1 = \sigma_2 = 1$. Numerically, the pressure difference is obtained on the domain $(0,1)\times(0,1)$ with the uniform grids $h = 1/2^n$ for $n = 5,\ 6,\ 7$, and 8. Table 1 shows the convergence of the pressure jump between the ambient fluid and inner droplet as we refine the mesh size. Fig. 3(b) and (c) show the pressure field over the domain and along the line $y = 0.5$, respectively.

4.2. Dynamics of compound droplet in two dimensions

We introduce the Taylor deformation number defined for a simple droplet (Taylor, 1932) (see Fig. 4(a)), namely, $D = (L-B)/$

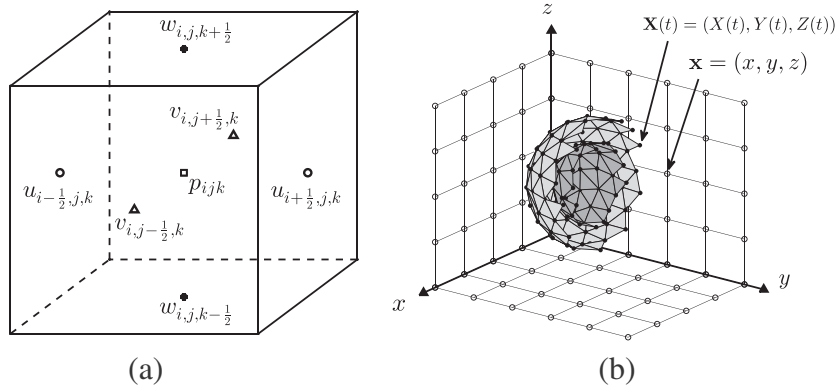

Fig. 2. (a) Velocities are defined at the cell interfaces, pressure is defined at the cell centers. (b) Eulerian points $\mathbf{x}$ and Lagrangian points $\mathbf{X}(t)$.

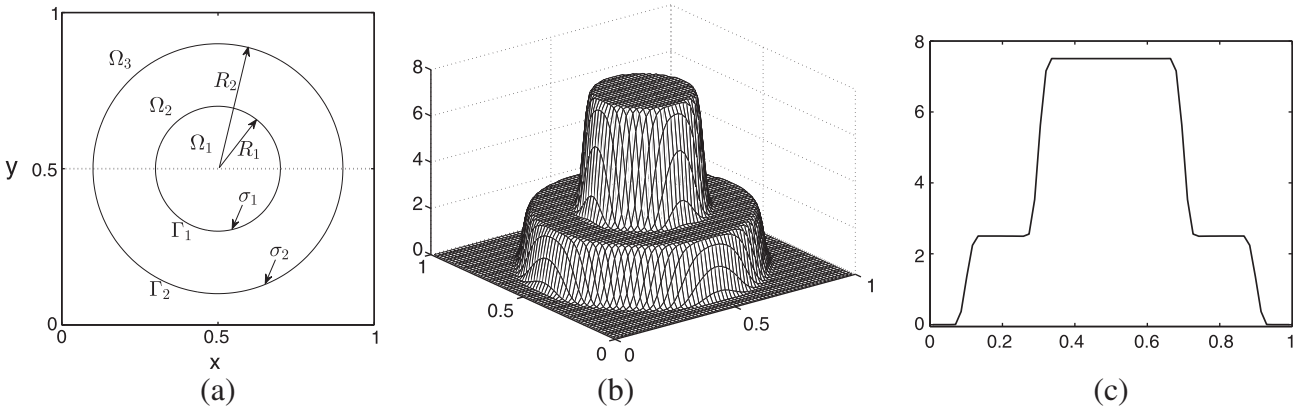

Fig. 3. (a) Schematic illustration of a drop-in-drop surrounded by ambient fluid. (b) Pressure field for the compound drop. (c) Slice of the pressure field at $y = 0.5$ (dotted line in (a)).

Table 1
Numerical pressure jump between the ambient fluid and the inner droplet with different mesh sizes. The theoretical pressure jump is 7.5.

Mesh size (h)	1/32	1/64	1/128	1/256
Numerical pressure jump	7.5089	7.5051	7.5045	7.5036

$(L + B)$, where L and B are the instantaneous maximum and minimum distances of the drop from its center, respectively. The inclination angle θ is defined as the angle between the long axis L and the x-axis. For the compound case, Fig. 4(b) illustrates the inclination angles θ_1 and θ_2 for the inner and outer interfaces, respectively. Let R, R_1, and R_2 be the radii of the simple, inner, and outer droplet, respectively.

4.2.1. Effect of radius ratio

Let $R = R_2$, where R is the simple droplet radius and R_2 is the outer droplet radius of a compound droplet. We increase the inner droplet radius of the compound droplet to examine the effect of inner droplet size on the deformation of the outer droplet. The computational domain is $\Omega = (-6, 6) \times (-3, 3)$, and a spatial step of $h = 6/128$ and time step of $\Delta t = 0.2h^2$ are used. Fig. 5(a) and (b) show the equilibrium shapes at $t = 10$ and the temporal evolution of the outer droplet's deformation for various values of the core droplet radius R_1. When $R_1 = 0.1$, the equilibrium morphology and the evolution of the deformation number D in the outer droplet of the compound droplet are almost identical to the simple binary droplet. With increased inner droplet sizes, B and L are getting larger and smaller, respectively.

4.2.2. Inclination angle of inner droplet

Fig. 6(a) shows a snapshot of the velocity field for a compound droplet when $t = 10$. The inner droplet undergoes a rotational velocity field inside the outer droplet. In this case, parameters $R_1 = 0.6$, $R_2 = 1$, $k = 0.6$, $\beta = 0.6$, $Re = 1$, $Ca_2 = 0.25$, and $Ca_1 = (k/\beta)Ca_2$ are used. Here, $k = R_1/R_2$ and $\beta = \sigma_1/\sigma_2$. Fig. 6(b) shows the temporal evolution of θ_1 and θ_2 for the compound droplet. We can observe that θ_1 is always greater than or equal to θ_2.

4.2.3. Eccentric compound droplet

We next investigate the behavior of the compound droplet when the initial inner droplet is eccentrically located in the shear flow. We set $\Omega = (-6, 6) \times (-3, 3)$, $h = 6/128$, $\Delta t = 0.2h^2$, $R_1 = 0.5$, $R_2 = 1$, $k = 0.5$, $\beta = 1$, $Re = 1$, $\dot{\gamma} = 1$, and $Ca_2 = 0.25$. The centers of the inner droplets are initially located at $(-1/4, 0)$, $(-\sqrt{2}/8, \sqrt{2}/8)$, $(0, 1/4)$, and $(\sqrt{2}/8, \sqrt{2}/8)$, as shown in the first row of Fig. 7. The second row of Fig. 7 shows the shapes and positions of the compound droplets in the steady state after the centers have been horizontally shifted. We can see that there is almost no difference in the droplet shapes for different initial positions.

4.3. Dynamics of compound droplet in three dimensions

In this section, we investigate the effects of the radius ratio, interfacial tension ratio, Ca number, and wall confinement on the morphology of the compound droplet under shear flow in the steady state.

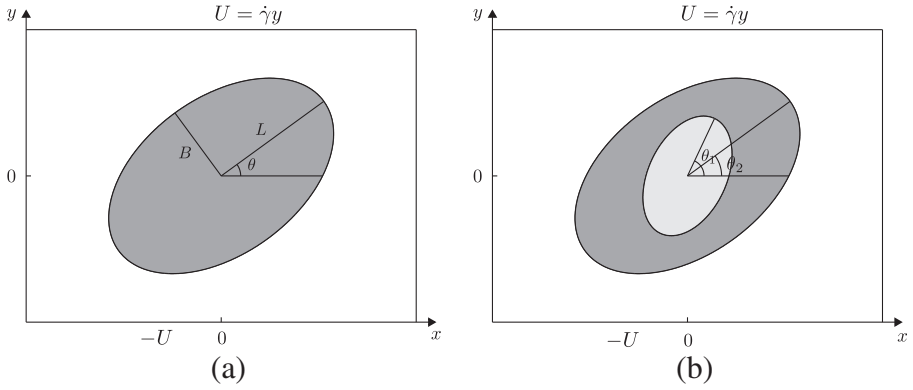

Fig. 4. Schematic representation: (a) maximum distance L, minimum distance B, and inclination angle θ. (b) Inclination angles θ_1 and θ_2 for the inner and outer interfaces of a compound droplet, respectively.

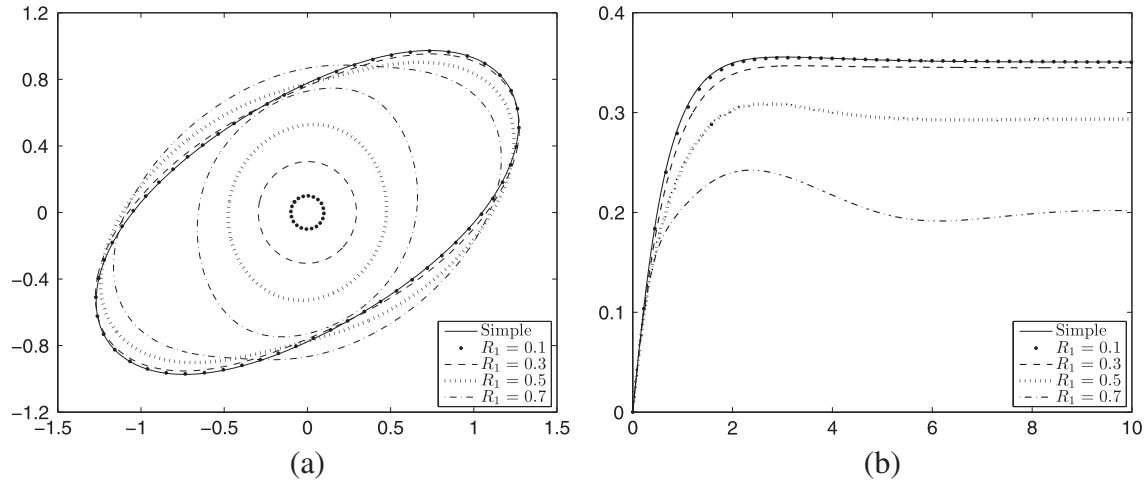

Fig. 5. (a) Shapes of simple and compound droplets when $t = 10$. (b) Temporal evolution of the outer droplet's deformation number with varying R_1.

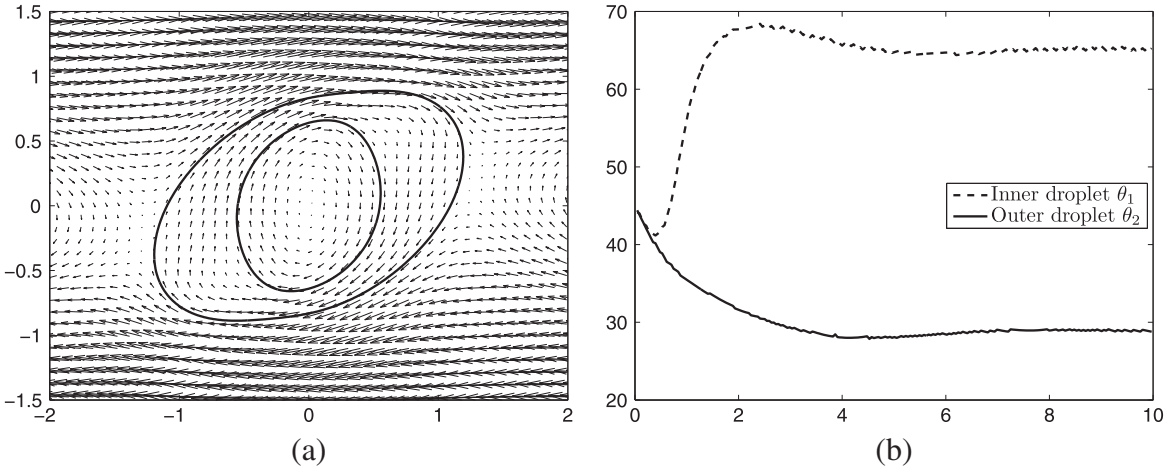

Fig. 6. (a) Velocity field of the compound drop in the steady state. (b) Temporal evolution of θ_1 and θ_2.

4.3.1. Effect of radius ratio

We increase the radius of the inner droplet to study its effect on the morphology of the outer droplet. The domain $\Omega = (-4,4)\times(-2,2)\times(-2,2)$, and parameter values of $h = 1/16$, $\Delta t = 0.1h^2$, $Re = 1$, $\beta = 1$, and $Ca_2 = 0.25$ are used. We fix the outer radius $R_2 = 1$ and change the inner radius $R_1 = kR_2$, where the radius ratio $k = 0.3,\ 0.5$, and 0.7. In addition, a value of $Ca_1 = (k/\beta)Ca_2$ is used. Fig. 8 shows the steady state shapes of compound droplets. The inner droplet strongly affects the deformation of the outer one as the radius ratio k increases. As in the two-dimensional case, the velocity field in the region enclosed by the outer droplet can be viewed as another induced shear flow for the inner droplet. The inclination of the inner droplet is based on this induced shear flow. When $k = 0.7$, the interfaces of the inner and outer droplets are closer to each other than in other cases; therefore, the inner droplet encounters a strong inclined shear flow, resulting in greater inclination toward the flow direction compared with the results for $k = 0.3$ and 0.5. In addition, the shape of the outer interface deviates further from the ellipsoidal shape as k increases.

4.3.2. Effect of interfacial tension ratio

To investigate the effect of surface tension, we fix the surface tension of the outer droplet and change that of the inner droplet. We set $\Omega = (-4,4)\times(-2,2)\times(-2,2)$, $R_1 = 0.5$, $R_2 = 1$, h=1/16, $\Delta t = 0.1h^2$, and $Re = 5$. First, we fix the capillary number of the outer droplet to $Ca_2 = 0.05$, and set $Ca_1 = (k/\beta)Ca_2$ with $\beta = 0.1,\ 0.05$, and 0.025 to decrease the interface tension of the inner droplet. Fig. 9 shows the steady-state shape of the compound droplet. The inner droplets become more stretched as the inner surface tension decreases. Furthermore, decreasing the surface tension of the inner droplet makes it more inclined to the direction of flow.

Next, we fix the capillary number of the inner droplet to $Ca_1 = 0.05$, and vary $Ca_2 = (\beta/k)Ca_1$ by setting $\beta = 0.5$, 1, and 2 to decrease the interface tension of the outer droplet. Fig. 10 shows the steady-state shapes of the compound droplets. As the outer surface tension decreases, the outer droplets become more stretched and inclined toward the flow direction. When $\beta = 2$, the shape of the outer interface deviates from an ellipsoid.

4.3.3. Comparison with a simple droplet

To study the effect of the capillary number of the outer droplet, we compare the results with those for a simple droplet. For the numerical simulations, we use $M = M_2 = 1896$ for the simple and outer droplets, and $M_1 = 462$ for the inner droplet. We set $\Omega = (-2H,2H)\times(-2H,2H)\times(-H,H)$, $R = R_2 = 1$, $R_1 = 0.5$, $H = 0.5/0.415$, and $\beta = 0.5$. The capillary number $Ca = Ca_2$ and Reynolds number $Re = 5Ca$ are then varied. Fig. 11 shows the simple and compound droplets in the steady state. In both cases, increasing Ca makes the droplets more stretched and inclined toward the fluid directions. However, the interaction between the inner and

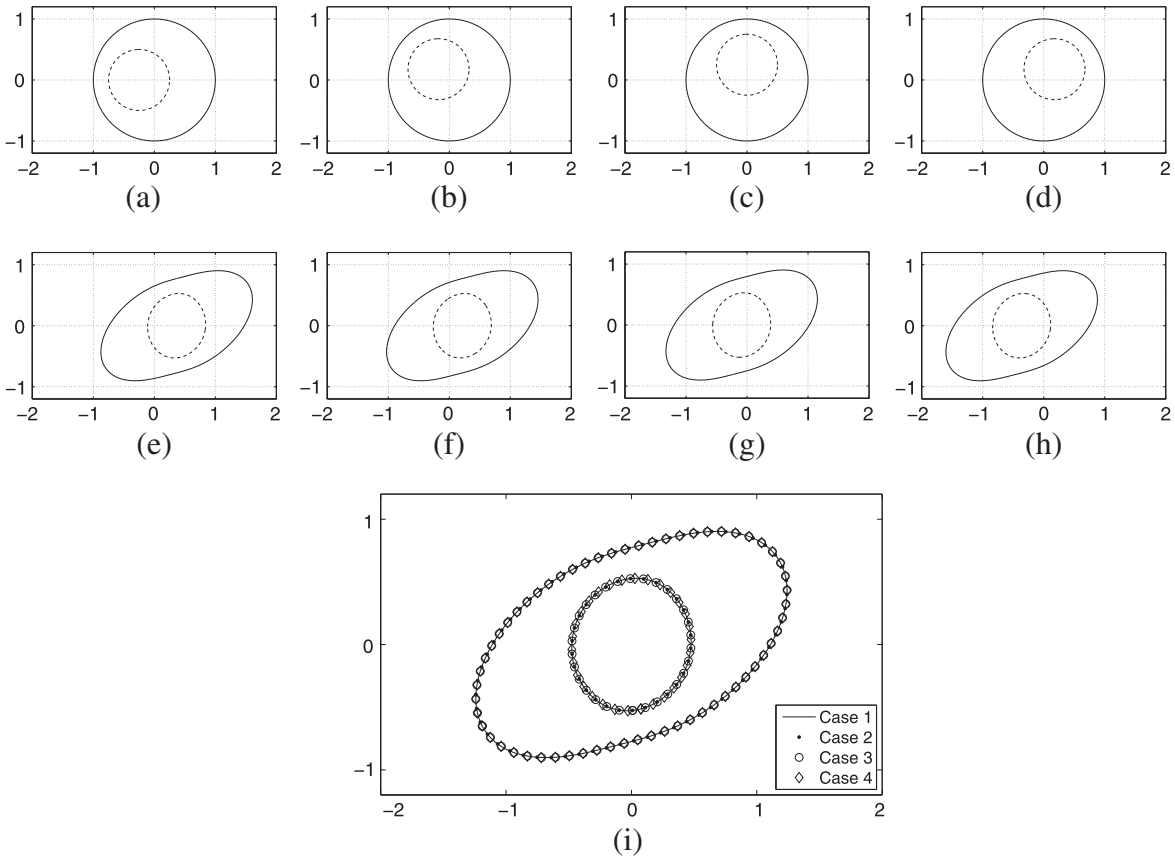

Fig. 7. Effect of inner droplet position on the shape of the compound droplet. Figures (a) to (d) illustrate the initial shapes, and figures (e) to (h) are the corresponding shapes in the steady state. (i) Overlapped interface of the steady-state shapes for the outer and inner droplets.

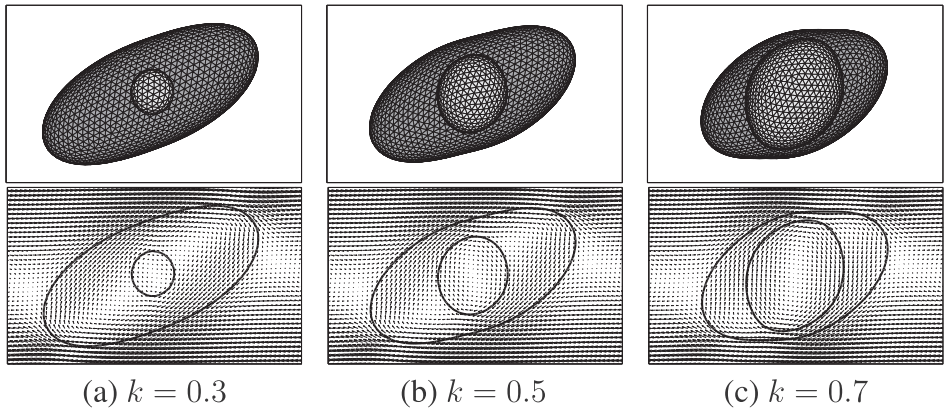

Fig. 8. Radius ratio effect of compound droplet. Top row: surface mesh viewed from x–z plane; bottom row: velocity vector field and interface of the compound droplet in the $y = 0$ plane.

outer droplets in the compound case makes the outer droplets less deformed than the simple droplets.

To compare the dynamics of the simple and compound cases, we consider the dimensionless axes L/R, B/R, and W/R with various capillary numbers. For the simple droplet, the effect of the capillary number has been studied theoretically in Minale (2008) and experimentally in Vananroye et al. (2007). For the numerical simulations, to match this experimental situation, we use a wall height of $H = 0.5/0.415$, outer radius $R_2 = R = 1$, and $Re = 5Ca$. In addition, we set the inner radius as $R_1 = 0.5$ for the compound case. Note that the viscosity ratio of the droplet and ambient fluid is 1.07 in the theoretical and experimental results, whereas we use a unit viscosity in our numerical simulations. Fig. 12 shows the experimental, numerical simulation, and theoretical results for various capillary numbers. In Fig. 12, the closed, dashed, and dotted lines represent the dimensionless axes L/R, B/R, and W/R from the theoretical analysis, respectively. The symbols denote corresponding values from the experiment and numerical simulations. When $Ca = 0.1$ and $Ca = 0.15$, all three approaches are in good agreement. For the smaller value of $Ca = 0.05$, the numerical results from the simple and compound droplets are almost the same. In the simple droplet case, the computational results lie between the experimental and theoretical results. For a larger value of $Ca = 0.25$, the dimensionless values

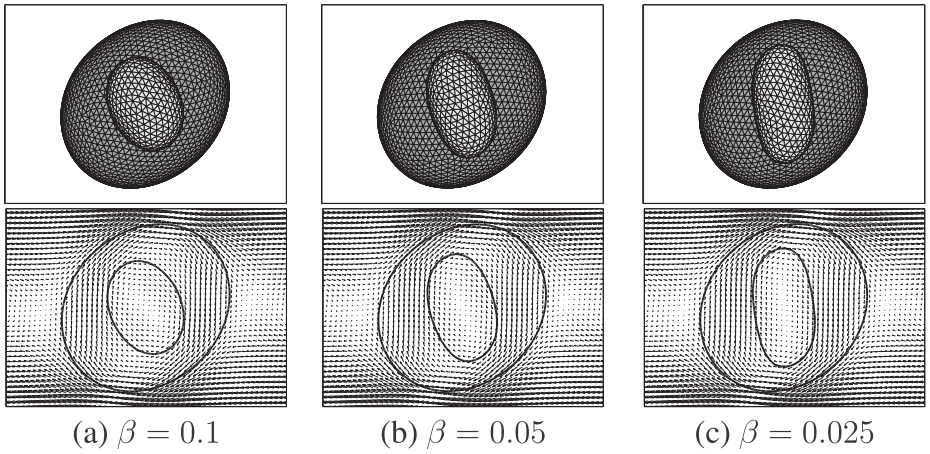

Fig. 9. Effect of inner droplet surface tension on the steady state of the compound droplet. First row illustrates the surface meshes viewed from x–z plane. Second row shows the vector field with contours at $y = 0$.

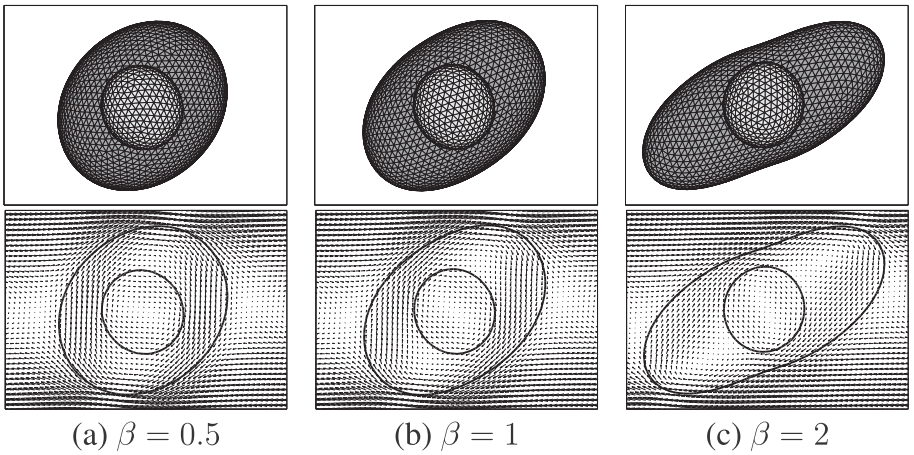

Fig. 10. Effect of outer droplet surface tension on the steady state of the compound droplet. First row illustrates the surface meshes viewed from x–z plane. Second row shows the vector field with contours at $y = 0$.

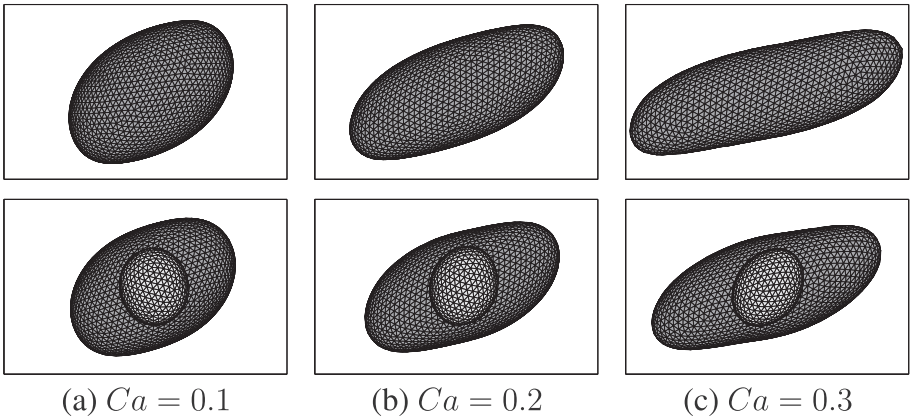

Fig. 11. Side views of the simple and compound droplets in the steady state. The first and second rows show simple and compound droplets, respectively.

from the compound droplet are different to those from the simple droplet. This is due to the existence of the inner droplet.

4.3.4. Effect of wall confinement

We study the wall effect on the hydrodynamics of the compound droplet, and compare its steady shape with the simple droplet under the same conditions. The computational domain is $(-3H, 3H) \times (-3H, 3H) \times (-H, H)$. We use wall heights of $H = 2$, 1.5, 1.25, 1, and 0.8. For the numerical simulations, we use $Re = 1$, $R = R_2 = 1$, $R_1 = 0.5$, $Ca = Ca_2 = 0.25$, and $\beta = 0.5$. Because of the case $H = 0.8$, the initial shapes are prolate ellipsoids that have the same volumes as with radii of R, R_1, or R_2. Fig. 13 shows a side view of the simple and compound droplets in the steady states. For the compound droplet, decreasing the wall height makes both

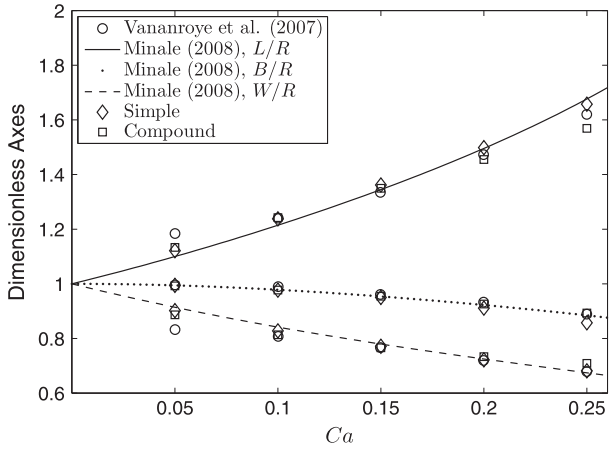

Fig. 12. Dimensionless axes for the simple and compound droplets versus *Ca* number.

outer and inner droplets more inclined toward the flow direction. This is similar to the behavior of the simple droplet. As the compound droplet becomes more confined, the shape difference compared with the simple droplet for the same wall height increases. The compound droplet is less elongated than the simple droplet.

5. Conclusions

The deformation dynamics of a compound liquid droplet in shear flow has been numerically investigated in two- and three-dimensional spaces. We extended a recently developed volume-conserving IBM for two-phase fluid flows to ternary compound droplet flows, and applied a surface remeshing algorithm for long time simulations. We studied the effects of radius, interfacial tension ratios, and inner droplet location on the deformation of a compound droplet. We computed the inclination angles of the inner and outer droplets. The simulation results indicate that the angle of the inner droplet is always greater than or equal to that

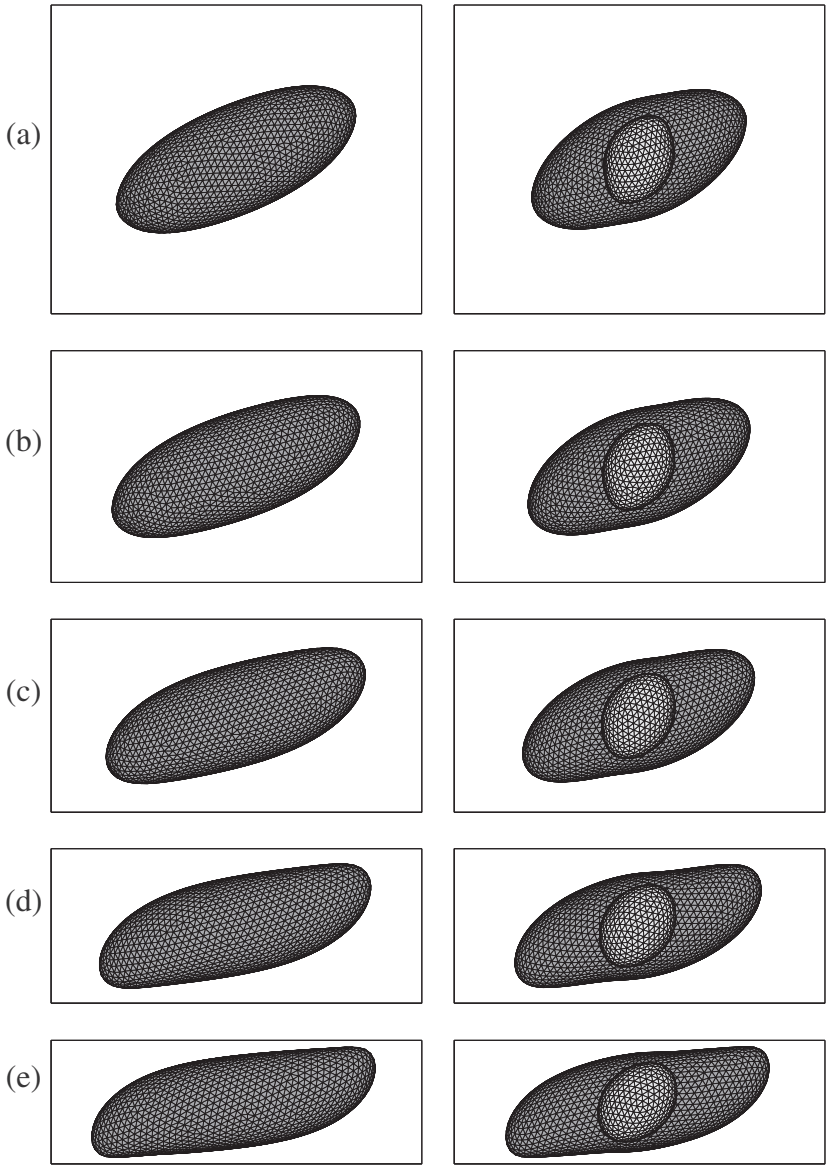

Fig. 13. Simple and compound droplets in the steady state with wall heights of: (a) $H = 2$, (b) $H = 1.5$, (c) $H = 1.25$, (d) $H = 1$, and (e) $H = 0.8$. Left and right columns show simple and compound droplet results, respectively.

of the outer one. The effect of wall confinement on compound droplet deformation was compared with that of a simple droplet. The results show that, as the wall becomes more confined, the difference in behavior between the compound and simple droplets increases. The novelties of this study are (i) the three-dimensional volume-conserving immersed boundary method and surface remeshing for a compound droplet, which enable accurate and stable simulations, (ii) our investigation of the influence of fluid properties, droplet sizes, and inner droplet locations, and (iii) our comparison of wall confinement effects with those of a simple droplet.

Acknowledgments

This research was supported by the Basic Science Research Program through the National Research Foundation of Korea (NRF), funded by the Ministry of Education (NRF-2011-0023794). The authors are grateful to the anonymous referees, whose valuable suggestions and comments significantly improved the quality of this paper.

References

Bartok, W., Mason, S.G., 1959. Particle motions in sheared suspensions: VIII. Singlets and doublets of fluid spheres. J. Colloid Sci. 14, 13–26.
Bazhlekov, I.B., Shopov, P.J., Zapryanov, Z.D., 1995. Unsteady motion of a type-A compound multiphase drop at moderate Reynolds numbers. J. Colloid Interface Sci. 169, 1–12.
Chen, R.-H., Chiu, S.-L., Lin, T.-H., 2007. Resident time of a compound drop impinging on a hot surface. Appl. Therm. Eng. 27, 2079–2085.
Choirn, A.J., 1968. Numerical solution of the Navier–Stokes equations. Math. Comput. 22, 745–762.
Gao, P., Feng, J.J., 2011. Spreading and breakup of a compound drop on a partially wetting substrate. J. Fluid Mech. 682, 415–433.
Harlow, F.H., Welch, J.E., 1965. Numerical calculation of time-dependent viscous incompressible flow with free surface. Phys. Fluids 8, 2182–2189.
Hinch, E.J., Acrivos, A., 1980. Long slender drops in a simple shear flow. J. Fluid Mech. 98, 305–328.
Hirofumi, S., Kuwabara, T., Kawano, S., Suzuki, T., Kanno, I., Kotera, H., 2007. Micro cell encapsulation and its hydrogel-beads production using microfluidic device. Microsyst. Technol. 13, 951–958.
Hua, H., Li, Y., Shin, J., Song, H., Kim, J., 2013. Effect of confinement on droplet deformation in shear flow. Int. J. Comput. Fluid D. 27, 317–331.
Janssen, P.J.A., Anderson, P.D., 2007. Boundary-integral method for drop deformation between parallel plates. Phys. Fluids 19, 043602-1–043602-11.
Johnson, R.E., Sadhal, S.S., 1985. Fluid mechanics of compound multiphase drops and bubbles. Annu. Rev. Fluid Mech. 17, 289–320.
Lai, M.C., Tseng, Y.H., Huang, H., 2008. An immersed boundary method for interfacial flows with insoluble surfactant. J. Comput. Phys. 227, 7279–7293.
Landau, L.D., Lifshitz, E.M., 1987. Fluid Mechanics. Butterworth-Heinemann, Oxford.
Li, Y., Yun, A., Lee, D., Shin, J., Jeong, D., Kim, J., 2013. Three-dimensional volume-conserving immersed boundary model for two-phase fluid flows. Comput. Methods Appl. Mech. Energy 257, 36–46.
Minale, M., 2008. A phenomenological model for wall effects on the deformation of an ellipsoidal drop in viscous flow. Rheol. Acta 47, 667–675.
Minale, M., 2010. Models for the deformation of a single ellipsoidal drop: a review. Rheol. Acta 49, 789–806.
Peskin, C.S., 1977. Numerical analysis of blood flow in the heart. J. Comput. Phys. 25, 220–252.
Peskin, C.S., McQueen, D.M., 1995. A general method for the computer simulation of biological systems interacting with fluids. Symp. Soc. Exp. Biol. 49, 265–276.
Pillapakkam, S.B., Singh, P., 2001. A level-set method for computing solutions to viscoelastic two-phase flow. J. Comput. Phys 174, 552–578.
Qu, X., Wang, Y., 2012. Dynamics of concentric and eccentric compound droplets suspended in extensional flows. Phys. Fluids 24, 123302-1–123302-21.
Renardy, Y., 2007. The effects of confinement and inertia on the production of droplets. Rheol. Acta 46, 521–529.
Renardy, Y.Y., Cristini, V., 2001. Effect of inertia on drop breakup under shear. Phys. Fluids 13, 7–13.
Rumscheidt, F.D., Mason, S.G., 1961. Particle motions in sheared suspensions XII. Deformation and burst of fluid drops in shear and hyperbolic flow. J. Colloid Sci. 16, 238–261.
Sheth, K.S., Pozrikidis, C., 1995. Effects of inertia on the deformation of liquid drops in simple shear flow. Comput. Fluids 24, 101–119.
Sibillo, V., Pasquariello, G., Simeone, M., Cristini, V., Guido, S., 2006. Drop deformation in microconfined shear flow. Phys. Rev. Lett. 97, 054502-1–054502-4.
Smith, K.A., Ottino, J.M., Olvera de la Cruz, M., 2004. Encapsulated drop breakup in shear flow. Phys. Rev. Lett. 93, 204501-1–204501-4.
Stone, H.A., Leal, L.G., 1990. Breakup of concentric double emulsion droplets in linear flows. J. Fluid Mech. 211, 123–156.
Tasoglu, S., Kaynak, G., Szeri, A.J., Demirci, U., 2010. Impact of a compound droplet on a flat surface: a model for single cell epitaxy. Phys. Fluids 22, 082103-1–082103-15.
Taylor, G.I., 1932. The viscosity of a fluid containing small drops of another fluid. Proc. R. Soc. A 138, 41–48.
Taylor, G.I., 1934. The formation of emulsions in definable fields of flow. Proc. R. Soc. A 146, 501–523.
Torza, S., Cox, R.G., Mason, S.G., 1972. Particle motions in sheared suspensions XXVII. Transient and steady deformation and burst of liquid drops. J. Colloid Interface Sci. 38, 395–411.
Trottenberg, U., Oosterlee, C.W., Schüller, A., 2001. Multigrid. Academic Press, UK, USA.
Utada, A.S., Lorenceau, E., Link, D.R., Kaplan, P.D., Stone, H.A., Weitz, D.A., 2005. Monodisperse double emulsions generated from a microcapillary device. Science 308, 537–541.
Vananroye, A., Van Puyvelde, P., Moldenaers, P., 2007. Effect of confinement on the steady-state behavior of single droplets during shear flow. J. Rheol. 51, 139–153.
Vananroye, A., Janssen, P.J.A., Anderson, P.D., Puyvelde, P.V., Moldenaers, P., 2008. Microconfined equiviscous droplet deformation: comparison of experimental and numerical results. Phys. Fluids 20, 013101-1–013101-10.
Yue, P., Feng, J.J., Liu, C., Shen, J., 2004. A diffuse-interface method for simulating two-phase flows of complex fluids. J. Fluid Mech. 515, 293–317.
Yue, P., Zhou, C., Feng, J.J., Ollivier-Gooch, C.F., Hu, H.H., 2006. Phase-field simulations of interfacial dynamics in viscoelastic fluids using finite elements with adaptive meshing. J. Comput. Phys. 219, 47–67.